Analysing protein post-translational modform regions by linear programming

Deepesh Agarwal[1,*], Ryan T. Fellers [2,*], Bryan P. Early[2,*], Dan Lu[1], Caroline J. DeHart[2], Philip D. Compton[2], Paul M. Thomas[2], Galit Lahav[1], Neil L. Kelleher[2], and Jeremy Gunawardena[1,†]

[1]Department of Systems Biology, Harvard Medical School, Boston, MA 02111, USA
[2]National Resource for Translational and Developmental Proteomics, Northwestern University, Evanston, IL 60208, USA
[*]These authors contributed equally
[†]Corresponding author: Jeremy Gunawardena (jeremy@hms.harvard.edu)

Post-translational modifications (PTMs) at multiple sites can collectively influence protein function but the scope of such PTM coding has been challenging to determine. The number of potential combinatorial patterns of PTMs on a single molecule increases exponentially with the number of modification sites and a population of molecules exhibits a distribution of such "modforms". Estimating these "modform distributions" is central to understanding how PTMs influence protein function. Although mass-spectrometry (MS) has made modforms more accessible, we have previously shown that current MS technology cannot recover the modform distribution of heavily modified proteins. However, MS data yield linear equations for modform amounts, which constrain the distribution within a high-dimensional, polyhedral "modform region". Here, we show that linear programming (LP) can efficiently determine a range within which each modform value must lie, thereby approximating the modform region. We use this method on simulated data for mitogen-activated protein kinase 1 with the 7 phosphorylations reported on UniProt, giving a modform region in a 128 dimensional space. The exact dimension of the region is determined by the number of linearly independent equations but its size and shape depend on the data. The average modform range, which is a measure of size, reduces when data from bottom-up (BU) MS, in which proteins are first digested into peptides, is combined with data from top-down (TD) MS, in which whole proteins are analysed. Furthermore, when the modform distribution is structured, as might be expected of real distributions, the modform region for BU and TD combined has a more intricate polyhedral shape and is substantially more constrained than that of a random distribution. These results give the first insights into high-dimensional modform regions and confirm that fast LP methods can be used to analyse them. We discuss the problems of using modform regions with real data, when the actual modform distribution will not be known.

1 INTRODUCTION

2 Post-translational modifications are ubiquitous on most proteins and greatly increase the number of "proteoforms"

3 which participate in cellular processes [1]. Certain modifications require carrier molecules which donate the modifying

4 moiety and enzymes to regulate both forward modification and reverse demodification [19, 27]. Phosphorylation on

5 S, T or Y residues, for example, requires ATP as the carrier molecule and enzymatic regulation is undertaken by

6 protein kinases and phospho-protein phosphatases. Background cellular processes maintain the concentrations of

7 carrier molecules, thereby acting like a chemical battery to drive the modifying reactions. This energy-dissipating

8 architecture confers a distinctive regulatory capability on such reversible, enzymatically-regulated post-translational

9 modifications (hereafter, "PTMs") [19], on which we will focus in this paper.

10 Proteins are often modified on multiple amino-acid residues (sites) as well as by different kinds of PTMs. For

11 instance, the transcription factor and "guardian of the genome", p53, is known to be modified on over 100 sites [4].

12 If these PTMs were all binary modifications, which would either be present or absent, then the number of potential

13 combinatorial patterns of modification on a single p53 molecule is $2^{100} \approx 1.3 \times 10^{30}$. This illustrates the extraordinary

14 PTM complexity that can surround even a single cellular protein. Of course, not all these patterns of modification can

15 be present at any one time but that only begs the question of which patterns are present and what their functions are.

16 Since PTMs effectively replace amino acids by different chemical residues, it is not surprising that they influence

17 protein function. It is not just PTM at a single site but also the pattern of PTMs across an entire protein molecule which

18 can modulate what that molecule does. There is now evidence from many biological contexts of extensive crosstalk

19 between different modified sites [9, 14, 20, 25, 7]. This has suggested the existence of PTM "codes" [2, 13, 26, 15,

20 17, 6, 16, 8, 24, 11]. The histone code is the best known [8, 24] but p53 itself exhibits complex PTM "barcodes"

21 which determine its varied responses in different cellular circumstances [15]. In this conceptual picture, upstream

22 enzymes "write" and "erase" modifications on a target protein to create "codewords", which are subsequently "read"

23 by downstream processes. While this idea of information encoding is attractive [19], it has been challenging to confirm

24 the biochemical details in any context. In view of the key role played by PTMs in so many cellular processes, clarifying

25 how PTMs process information has become a central problem of systems biology.

26 We have previously introduced a quantitative language for analysing this problem [18, 19]. We refer to a combi-

27 natorial pattern of PTMs across a single protein molecule as a "modform". As noted above, the number of potential

28 modforms increases exponentially with the number of modification sites. A given protein will be present within a cell

29 as a population of single molecules and each molecule can, in principle, exhibit its own modform. The most compre-

30 hensive measure of the protein's PTM state is therefore given by the abundance of each modform in the population,

31 which we call the "modform distribution". This can be thought of as a histogram over the modforms or as a point in

32 a high-dimensional space, in which each dimension, or coordinate axis, corresponds to a specific modform (Fig.1).

33 If we are to determine how information is encoded by PTMs, then estimating a protein's modform distribution, at a

34 given time and in a given biological context, is essential. This is the main concern of the present paper.

35   There are a limited number of methods for measuring PTMs. Modification-specific antibodies have been of great

36 importance and have unrivalled sensitivity, including at single-cell level through immunostaining. However, at best,

37 they can only detect PTMs on nearly adjacent sites and are oblivious to the overall modform. Moreover, in comparison

38 to other methods, their quantitative accuracy is suspect [18]. Nuclear magnetic resonance spectroscopy (NMR) is

39 highly quantitative and can reveal certain modform features as well as interactions with binding partners [10, 18] but

40 the limitation to bulk in-vitro measurements has only recently been lifted [12]. Mass spectrometry (MS) remains, at

41 present, the method of choice for estimating modform distributions [18].

42   In the most-widely used "bottom-up" MS (BU MS), proteins are first proteolytically cleaved into peptides before

43 chromatographic separation and mass determination [21]. So-called "middle-down" MS (MD MS) uses fewer cleav-

44 ages and correspondingly larger peptides [23]. Peptide modforms can be partly resolved during chromatography and

45 further determined by rounds of fragmentation (MS^n) in the spectrometer, allowing peptide modform distributions

46 to be estimated. However, cleavage severs correlations between modforms on different peptides, leaving the protein

47 modform distribution undetermined [18]. It has seemed conceivable that with multiple proteases with different cleav-

48 age patterns, it might still be feasible to reconstruct the protein modform distribution. However, we recently showed

49 mathematically that this is impossible, no matter how many cleavage patterns and proteases are available and that,

50 furthermore, the shortfall in information required to determine the modform distribution increases exponentially with

51 the number of modification sites [3].

52   Although not yet so widely used, MS can now be undertaken on an intact protein by "top-down" MS (TD MS),

53 which maintains correlations across the protein [22]. It is harder to separate protein modforms by chromatography

54 but isobaric modforms, such as positional isomers, can be isolated within the spectrometer, thereby simplifying the

55 analysis. Fragmentation (MS^n) can again help to determine modforms but is more difficult to undertake with good

56 coverage for intact proteins. With current TD MS technologies, which rarely go beyond MS^3, the information shortfall

57 required to determine the modform distribution is reduced but still increases exponentially [3].

58   An alternative approach to estimating the modform distribution arises from realising that all MS methods lead to

59 linear equations in the modform amounts [3]. For example, suppose that the amounts of modforms 1 to 16 in Fig.1 are

60 $x_1, \cdots, x_{16}$. These are the coordinates of the modform distribution in the 16-dimensional modform space. If BU MS

61 is undertaken with a protease which cleaves between the second and third sites and the modform of the first peptide in

62 which both first and second sites are occupied (blue and magenta colours) is measured, then it follows that,

$$x_6 + x_{12} + x_{13} + x_{16} = A \,,$$

3

63 where A is the amount of the peptide modform. The protein modforms numbered 6, 12, 13 and 16 contribute the

64 appropriate peptide modform after cleavage, while the other protein modforms do not. Similarly, if we assume that

65 each colour in Fig.1 represents a PTM with a different mass, then it is possible to determine by TD MS the total

66 amount of those protein positional isomers with, for instance, one blue and one green PTM. This yields the equation,

$$x_7 + x_{11} = B\,, \tag{1}$$

67 where B is the total amount. These linear equations cannot determine the modform region, as noted above, but

68 they do constrain it, especially when taken together with the requirement that amounts cannot be negative, so that

69 $x_1, \cdots, x_{16} \geq 0$. For instance, this implies from Eq.1 that $0 \leq x_7 \leq B$. Additional equations may constrain this

70 range still further [18]. The totality of equations arising constrain the modform distribution to lie within a bounded

71 region in the high-dimensional space of all modforms (Fig.1, right). Because of the linearity of the equations, this

72 region must be convex and polyhedral. We refer to it as the "modform region". The high-dimensional shape of this

73 region can be informative as to which modforms dominate the population. By perturbing the cellular conditions,

74 the change in shape of the region can tell us which PTMs are implicated. It may then become feasible to test how

75 information is being represented by PTMs across the entire protein and to thereby unravel the nature of PTM coding.

76 The modform region can be thought of as a data-centric proxy for the modform distribution.

77   With that idea in mind, the present paper puts forward a methodology for approximately estimating the shape

78 of the modform region from MS data. It is based on linear programming, which offers an efficient algorithm for

79 determining optimum solutions to linear equations or inequalities. We describe the approach and show how it works

80 with simulated data. This gives the first insights into high-dimensional modform regions. We discuss the problems of

81 using these methods on actual data.

RESULTS

82

Linear equations for MS methods

83

84 It is necessary to have a systematic way to generate the linear equations described above. In previous work, we

85 introduced a mathematical formalism for doing so [3] but this was restricted to binary modifications, such as phos-

86 phorylation, which are either present or absent. This restriction permits a modform to be identified with the subset

87 of modified sites. Here, we extend the formalism to allow for more complex modifications [19, 27]. We explain the

88 formalism in generality but, for clarity of exposition, focus on those PTMs which are most relevant to the data acquired

89 below. A more complete treatment will be given subsequently. We use set theory notation, as explained in [3], which

90 may be consulted for more background.

4

91   Suppose that a protein has n sites of modification (hereafter, "sites"), indexed $1, \cdots, n$ in order from, say, the

92   N-terminus. Let $S = \{1, \cdots, n\}$ be the set of sites. Because different PTMs target different amino-acid residues, it is

93   necessary to keep track of which residue occurs at which site. Let $\mathcal{A}$ denote the set of relevant amino-acid residues.

94   For instance, if only phosphorylation is being considered, we might take $\mathcal{A} = \{S, T, Y\}$, using the customary one-

95   letter codes for amino-acids. We note that phosphorylation may also occur on H and E [19] but ignore that here for

96   simplicity. Let $\rho : S \to \mathcal{A}$ be the residue map, which assigns to each site $i \in S$, the corresponding amino-acid residue,

97   $\rho(i) \in \mathcal{A}$. This residue map is a property of the particular protein under study.

98   We now specify PTMs and define modforms. Let $\mathcal{M}$ denote the set of relevant, structurally-distinct PTMs, in-

99   cluding 0 for the absence of modification. For instance, if acetylation and methylation are being considered, then

100 $\mathcal{M} = \{0, \text{Ac}, \text{Me}, \text{Me2}, \text{Me3}\}$, using the customary abbreviations for PTMs. Polymeric modifications, such as ubiq-

101 uitination and ADP-ribosylation, present a complication, as the number of distinct structures may be unbounded and

102 must be indexed in some manner [19]. In principle, this could be done but the details are beyond the scope of the

103 present paper and we ignore such PTMs here for simplicity. We can think of a protein modform as a function,

104 $\chi : S \to \mathcal{M}$, which assigns to a site $i \in S$, the corresponding PTM, $\chi(i) \in \mathcal{M}$. However, such an assign-

105 ment must be consistent with the residue map ρ. The precise consistency requirement will depend on $\mathcal{A}$, $\mathcal{M}$ and

106 ρ but if we consider as an example phosphorylation, acetylation and methylation, so that $\mathcal{A} = \{S, T, Y, K\}$ and

107 $\mathcal{M} = \{0, P, \text{Ac}, \text{Me}, \text{Me2}, \text{Me3}\}$, then for $\chi : S \to \mathcal{M}$ to be consistent as a modform, it is necessary that

$$
\begin{aligned}
&\text{if } \chi(i) = P \text{ then } \rho(i) \in \{S, T, Y\} \\
&\text{if } \chi(i) \in \{\text{Ac}, \text{Me}, \text{Me2}, \text{Me3}\} \text{ then } \rho(i) = K \,.
\end{aligned}
\tag{2}
$$

108 Other consistency conditions can be readily formulated depending on the PTMs being considered. We will say that

109 the function χ is consistent and write $\chi : S \to_\rho \mathcal{M}$ if χ satisfies the appropriate consistency conditions with respect

110 to ρ, as in Eq.2, for the PTMs under consideration. We can now identify modforms with the consistent χ's. They can

111 be visualised as in the following example modform on 8 sites,

$$
\begin{array}{cccccccc}
1(\text{K}) & 2(\text{S}) & 3(\text{S}) & 4(\text{K}) & 5(\text{Y}) & 6(\text{T}) & 7(\text{K}) & 8(\text{K}) \\
\downarrow & \downarrow & \downarrow & \downarrow & \downarrow & \downarrow & \downarrow & \downarrow \\
\text{Ac} & 0 & P & \text{Me3} & P & P & 0 & \text{Me2}\,.
\end{array}
\tag{3}
$$

112 Eq.3 makes clear the resemblance between the modform as defined here and the representation that is often used

113 in the literature, in which the sequence of modifications are listed, K1Ac.S3P.K4Me3.Y5P.T6P.K8Me2. When the

114 sites are known, it is more convenient to denote this Ac.0.P.Me3.P.P.0.Me2 and we will use that format below. The

115 number of potential modforms can be calculated from the consistency conditions. For instance, for the example just

116 considered, the consistency conditions in Eq.2 imply that there are 2 possibilities for the modification state of S, T

117 and Y and 5 possibilities for the modification state of K, so that the total number of combinatorial possibilities is

118 $5 \times 2 \times 2 \times 5 \times 2 \times 2 \times 5 \times 5 = 2^4 5^4 = 10000$.

119   If we only consider a binary modification like phosphorylation, so that $\mathcal{M} = \{0, \mathrm{P}\}$, then the function $\chi : S \to \mathcal{M}$

120 can be identified with the subset of modified sites, $\{i \in S \,|\, \chi(i) = P\}$. Sets were sufficient for our previous work,

121 which involved only such binary modifications [3]. For the more complex modifications considered here, we need

122 functions, $\chi : S \to \mathcal{M}$.

123   Let $\mathbb{M}(S)$ denote the set of protein modforms, $\mathbb{M}(S) = \{\chi : S \to_\rho \mathcal{M}\}$. A modform distribution is an assignment

124 to each modform of an amount. This corresponds to a function, $x : \mathbb{M}(S) \to \mathbb{R}$, from the set of modforms to the real

125 numbers, $\mathbb{R}$. Here, $x(\chi)$ is the amount of modform χ, which corresponds to the height of the corresponding bar in

126 the modform histogram in Fig.1. Since amounts are non-negative, $x(\chi) \geq 0$, for all χ (which we will write $x \geq 0$).

127 The functions $\mathbb{M}(S) \to \mathbb{R}$ form a vector space, which we will denote $\mathbb{R}^{\mathbb{M}(S)}$ [3]. The dimension of this vector space

128 is given by the number of protein modforms, or the size of $\mathbb{M}(S)$. If X is any finite set, its size will be denoted $\#X$,

129 and we will use N to denote the number of protein modforms, so that $N = \#\mathbb{M}(S)$. A standard basis for $\mathbb{R}^{\mathbb{M}(S)}$ is

130 provided by the unit vectors corresponding to each modform, which lie on the coordinate axes in the modform space

131 in Fig.1. Let $e(\chi) \in \mathbb{R}^{\mathbb{M}(S)}$ denote the unit vector corresponding to the modform χ. As a function on $\mathbb{M}(S)$,

$$e(\chi)(\chi_1) = \begin{cases} 1 & \text{if } \chi = \chi_1 \\ 0 & \text{otherwise} \end{cases} \tag{4}$$

132 and a modform distribution can be expressed as a linear combination of these basis vectors,

$$x = \sum_{\chi \in \mathbb{M}(S)} x(\chi) e(\chi) \,.$$

133   Up to now, we have discussed protein modforms, defined on the entire subset $S = \{1, \cdots, n\}$, but the same

134 notation may be used for any segment of the protein that arises through cleavage or fragmentation. Modification sites

135 on the segment are given the same indices as they have in the protein—the protein determines the universe in which

136 the segments are considered—so that a segment can be identified with a subset of sites, $T \subseteq S$. This segment has

137 corresponding segment modforms in $\mathbb{M}(T)$. It will be convenient to refer to modforms in $\mathbb{M}(T)$ as T-modforms, so

138 that protein modforms are S-modforms.

139   Cleavage or fragmentation are two of the basic procedures in mass-spectrometry, out of which many mass-

140 spectrometry experiments are built up. The effect of these procedures is described by a linear segment function,

141 $c_{S_1} : \mathbb{R}^{\mathbb{M}(S)} \to \mathbb{R}^{\mathbb{M}(T)}$, which takes S-modforms to T-modforms. This function is defined on basis vectors by restric-

6

142   tion of the function. If $f : X \to Y$ is a function and $X_1 \subseteq X$, then the restriction of f to S_1, denoted $f|_{X_1}$, is just the

143   composition $X_1 \subseteq X \xrightarrow{f} Y$. If $\chi \in \mathbb{M}(S)$, then the segment function is given by,

$$c_T(e_\chi) = e_{\chi|_T} \, .$$

144   Since this linear function takes a basic vector to a basis vector, its corresponding matrix has entries which are either

145   0 or 1. Consider, for example, $S = \{1, 2, 3\}$, $\rho(1) = \rho(2) = S$, $\rho(3) = K$, and $\mathcal{M} = \{0, P, Me, Me2, Me3\}$. There

146   are $2.2.4 = 16$ S-modforms. The segment corresponding to the subset $T = \{2, 3\}$ has 8 T-modforms. The process of

147   cleavage or fragmentation that creates T yields the segment function, c_T, whose 8×16 matrix is given by,

	0.0.0	0.0.Me	0.0.Me2	0.0.Me3	0.P.0	0.P.Me	0.P.Me2	0.P.Me3	P.0.0	P.0.Me	P.0.Me2	P.0.Me3	P.P.0	P.P.Me	P.P.Me2	P.P.Me3
0.0	1	0	0	0	0	0	0	0	1	0	0	0	0	0	0	0
0.Me	0	1	0	0	0	0	0	0	0	1	0	0	0	0	0	0
0.Me2	0	0	1	0	0	0	0	0	0	0	1	0	0	0	0	0
0.Me3	0	0	0	1	0	0	0	0	0	0	0	1	0	0	0	0
P.0	0	0	0	0	1	0	0	0	0	0	0	0	1	0	0	0
P.Me	0	0	0	0	0	1	0	0	0	0	0	0	0	1	0	0
P.Me2	0	0	0	0	0	0	1	0	0	0	0	0	0	0	1	0
P.Me3	0	0	0	0	0	0	0	1	0	0	0	0	0	0	0	1

.   (5)

148   Here, the modforms of the standard basis vectors in $\mathbb{R}^{\mathbb{M}(S)}$ and $\mathbb{R}^{\mathbb{M}(T)}$ are listed on the top and left, respectively, in

149   the sequence format introduced above.

150   We have mathematically described cleavage and fragmentation as linear functions on intact proteins, with the

151   domain of the functions being $\mathbb{R}^{\mathbb{M}(S)}$. But fragmentation can also be carried out recursively on any segment, $T_1 \subseteq S$.

152   We can define corresponding segment functions on $\mathbb{R}^{\mathbb{M}(T_1)}$ in the following way. Note first that given any pair of

153   subsets, $T_1, T_2 \subseteq S$, for which $T_2 \subseteq T_1$, there is a natural embedding of the smaller vector space $\mathbb{R}^{\mathbb{M}(T_2)}$ in the larger

154   vector space $\mathbb{R}^{\mathbb{M}(T_1)}$. We can consider a T_2-modform, $\chi \in \mathbb{M}(T_2)$, as if it were a T_1-modform by setting all sites in

155   T_1 which are outside T_2 to have no modification. In other words, we define, $\nu : \mathbb{M}(T_2) \to \mathbb{M}(T_1)$ by, for all $i \in T_1$,

$$\nu(\chi)(i) = \begin{cases} \chi(i) & \text{if } i \in T_2 \\ 0 & \text{otherwise} \, . \end{cases}$$

156   This function $\nu : \mathbb{M}(T_2) \to \mathbb{M}(T_1)$ defines an embedding of $\mathbb{M}(T_2)$ inside $\mathbb{M}(T_1)$. In turn, ν yields an embedding of

157   $\mathbb{R}^{\mathbb{M}(T_2)}$ inside $\mathbb{R}^{\mathbb{M}(T_1)}$, which is defined on basis vectors by sending e_χ to $e_{\nu(\chi)}$ for each T_2-modform $\chi \in \mathbb{M}(T_2)$. We

158   will denote this embedding, for any pair of subsets, $T_2 \subseteq T_1$, by $\mathbb{R}^{\mathbb{M}(T_2)} \hookrightarrow \mathbb{R}^{M(T_1)}$. Now, if $T_2 \subseteq T_1$ is considered

159   to be a fragment of T_1, we can define the T_2-segment function on T_1-modforms by the composition

$$\mathbb{R}^{\mathbb{M}(T_1)} \hookrightarrow \mathbb{R}^{\mathbb{M}(S)} \xrightarrow{c_{T_2}} \mathbb{R}^{\mathbb{M}(T_2)} \, .$$

7

160   We will denote this composition, with some abuse of notation, also by $c_{T_2} : \mathbb{R}^{\mathbb{M}(T_1)} \to \mathbb{R}^{\mathbb{M}(T_2)}$.

161   Cleavage or fragmentation may result in identification and measurement of the segment modforms. This may

162   come about through separation prior to MS or through further fragmentation within the spectrometer or both. In such

163   cases, the end result is an estimate of the modform distribution of the segment, for which matrices like those in Eq.5

164   give the necessary linear equations. It is also possible that only MS1 is undertaken on the segment. MS1 can resolve

165   modforms with different masses but is unable to resolve isobaric modforms with the same mass. This can be an issue

166   for individual PTMs: the nominal mass of phosphate (80 Da) is the same as that of sulphate and that of acetyl (42 Da)

167   is the same as that of tri-methyl (3×14). Modern spectrometers, which are accurate to a few parts per million, can

168   resolve the actual mass differences between such PTMs if the segment is not too large. However, they cannot resolve

169   positional isomers. We will deal with the case of positional isomers here. Extending the formalism to cover isobaric

170   modforms is straightforward but requires more notation.

171   The target of the resulting linear function is no longer a vector space of the kind $\mathbb{R}^{\mathbb{M}(T)}$. To describe it, let

172     $\chi_1 \sim \chi_2$ denote that the modforms $\chi_1, \chi_2 \in \mathbb{M}(S)$ are positional isomers. The precise definition depends on the

173   PTMs involved and care has to be taken with those like methylation which have multiple valencies. If $m \in \mathcal{M}$ and

174     $\chi \in \mathbb{M}(S)$, let $n_m(\chi)$ denote the number of sites having modification m, $n_m(\chi) = \#\{i \in S \,|\, \chi(i) = m\}$. If, for

175   instance, $\mathcal{M} = \{0, \mathrm{P}, \mathrm{Ac}, \mathrm{Me}, \mathrm{Me2}, \mathrm{Me3}\}$, then, $\chi_1 \sim \chi_2$ if, and only if,

$$
\begin{aligned}
n_{\mathrm{P}}(\chi_1) &= n_{\mathrm{P}}(\chi_2) \\
n_{\mathrm{Ac}}(\chi_1) &= n_{\mathrm{Ac}}(\chi_2) \\
n_{\mathrm{Me}}(\chi_1) + n_{\mathrm{Me2}}(\chi_1) + n_{\mathrm{Me3}}(\chi_1) &= n_{\mathrm{Me}}(\chi_2) + n_{\mathrm{Me2}}(\chi_2) + n_{\mathrm{Me3}}(\chi_2)
\end{aligned}
$$

176   It is clear that the relation $\sim$ is an equivalence relation on modforms and we can therefore form the set of equivalence

177   classes, $\mathbb{I}(S)$. Let $[\chi] \in \mathbb{I}(S)$ denote the equivalence class containing χ, $[\chi] = \{\chi_1 \in \mathbb{M}(S) \,|\, \chi_1 \sim \chi\}$, and let $e_{[\chi]}$ be

178   the corresponding standard unit vectors in $\mathbb{R}^{\mathbb{I}(S)}$, defined in a similar way to Eq.4. Then, MS1 measurement yields a

179   linear mass function, $i_S : \mathbb{R}^{\mathbb{M}(S)} \to \mathbb{R}^{\mathbb{I}(S)}$, from modforms to positional isomers, which is defined on basis vectors by,

$$
i_S(e_\chi) = e_{[\chi]} \,.
$$

180   It is straightforward to define positional isomers for any segment $T \subseteq S$, which yields the set $\mathbb{I}(T)$ and the corre-

181   sponding mass function, $i_T : \mathbb{R}^{\mathbb{M}(T)} \to \mathbb{R}^{\mathbb{I}(T)}$. As with cleavage or fragmentation, the resulting matrices, like that in

182   Eq.5, have entries which are 0 or 1.

183   Mass spectrometry experiments are typically composed of a sequence of the basic procedures of cleavage, frag-

184   mentation and MS1 measurement. For instance, the intact protein may be first cleaved by proteolytic digestion into the

185   segment $T_1 \subseteq S$, which is then fragmented into the segment $T_2 \subseteq T_1$, which is then subjected to MS1 measurement.

8

186   The overall effect on modforms is described by the linear function which is the composition of the corresponding

187   segment and mass functions,

$$\mathbb{R}^{\mathbb{M}(S)} \xrightarrow{c_{T_1}} \mathbb{R}^{\mathbb{M}(T_1)} \xrightarrow{c_{T_2}} \mathbb{R}^{\mathbb{M}(T_2)} \xrightarrow{i_{T_2}} \mathbb{R}^{\mathbb{I}(T_2)} \, . \tag{6}$$

188   The overall matrix for the composition can be obtained by multiplying the individual matrices. The dimension of the

189   overall matrix in this case is $\#\mathbb{I}(T_2) \times N$, with the number of columns always being the number of protein modforms,

190   as in Eq.5. Since the composition still sends basis vectors to basis vectors, the overall matrix still has entries which are

191   either 0 or 1. The overall matrices arising from each of the individual compositions of basic procedures can be abutted

192   "vertically" to form a single matrix, M, of size $r \times N$, where r is the total number of rows of the overall matrices taken

193   together. The matrix M summarises the outcome of whatever mass spectrometry experiments have been undertaken

194   as a system of linear equations for the unknown protein modform distribution, $x \in \mathbb{R}^{\mathbb{M}(S)}$,

$$M.x = d \, , \tag{7}$$

195   where d is the $r \times 1$ column vector of actual measurements.

196   There are other mass spectrometry procedures, such as isolating positional isomers prior to fragmentation [3]. It

197   is not difficult to define linear functions for these, in a similar way to what has been done above, but the procedures

198   described here cover many cases, including those needed for the simulations below. We now turn to asking what can

199   be determined from these linear equations.

Modform region estimation by linear programming

201   As shown previously, the system of linear equations given by Eq.7 is not sufficient to determine the unknown modform

202   distribution, $x \in \mathbb{R}^{\mathbb{M}(S)}$, [3] but it can be used to constrain the distribution within a region of $\mathbb{R}^{\mathbb{M}(S)}$ (Fig.1, right).

203   We can estimate this region by linear programming (LP). LP is about solving ("programming") the following type of

204   optimisation problem, for which we use the same notation as in Eq.7,

$$\begin{aligned} &\text{maximise (or minimise) } l(x) \\ &\text{subject to } M.x = d \\ &\text{and } x \geq 0 \end{aligned} \tag{8}$$

205   Here, x is a $N \times 1$ column vector of unknowns, $l(x)$ is a linear objective function of x, $l(x) = \sum_i l_i x_i$ for $l_i \in \mathbb{R}$,

206   which is specified below, M is the known $r \times N$ matrix in Eq.7 and d is the $r \times 1$ column vector of known data

207   values in Eq.7. Algorithms have been developed which allow LP problems with millions of unknowns to be solved

208   efficiently. This makes LP particularly attractive for modform region estimation, in which the number N of unknown

9

209   modform amounts may be extremely large.

210   The first requirement for using LP is that the problem should be feasible. In other words, there must be a value of x

211   which satisfies the linear system $M.x = d$. In our case, the value of d will be affected by several kinds of error, arising

212   from sample preparation, instrumentation and measurement, so it is possible that the linear system is infeasible. If so,

213   we first find the smallest perturbation of d which yields a feasible solution. The standard procedure is to introduce

214   for each data value, d_i, a pair of non-negative elastic, or slack, variables, $u_i \geq 0$ and $v_i \geq 0$, such that the vector of

215   perturbed data values, $d_i + u_i - v_i$ becomes feasible. We need two non-negative elastic variables because we may

216   sometimes have to increase d_i and sometimes have to decrease it. We can formulate this as an LP problem in which

217   we seek to minimse the total perturbation, $\sum_i (u_i + v_i)$, subject to the linear system,

$$(M \,|\, I_r \,|\, I_r) \begin{pmatrix} x \\ -u \\ v \end{pmatrix} = d \,,$$

218   and the inequality constraint $x, u, v \geq 0$. Here, we have extended x "vertically" by abutting the vectors $-u$ and v

219   to make an unknown vector of size $N + 2r$ and we have extended M "horizontally" by abutting two $r \times r$ identity

220   matrices, to make a matrix of size $r \times (N + 2r)$. It is easy to see that this linear system is equivalent to,

$$M.x = d + u - v \,,$$

221   as required. The solution of this LP problem allows us to replace the data vector d by the perturbed data vector

222    $d^* = d + u - v$, for which there is a feasible solution. By minimising the total perturbation, d^* is the most parsimonious

223   way to reach feasibility, from a linear perspective.

224   We now want to know the shape of the modform region defined by the feasible linear system $M.x = d^*$, with

225    $x \geq 0$. An approximate estimate of the shape can be obtained by using LP to find the minimum and the maximum of

226   each modform amount, x_i,

$$\text{maximise/minimise } x_i$$
$$\text{subject to } M.x = d^* \tag{9}$$
$$\text{and } x \geq 0 \quad .$$

227   This gives the range within which each modform amount falls, as optimally constrained by the MS data.

228   Range determination through this LP formulation has the advantage of being easy to undertake efficiently for large

229   N. However, it may provide a limited estimate of the actual modform region. For example, if the linear system

230   consists solely of Eq.1 in the Introduction, then the corresponding modform region is the line segment between the

231   points $(0, B)$ and $(B, 0)$ in Fig.2. However, the ranges of x_7 and x_{11} which come from Eq.9 are both $[0, B]$. This

232   would be same as if the modform region had been the square whose side length is B (Fig.2, magenta box). This is

233   also what happens in general: determination of each range by Eq.9 yields the smallest "hyper-rectangle" whose sides

234   are parallel to the coordinate axes and which contains the modform region (Fig.2). In the situation in Fig.2, the hyper-

235   rectangle is a "hyper-square", with equal sides, but this need not always be the case, as we will see. The individual

236   ranges do not reveal the coupling between x_7 and x_{11} which keeps the modform region one-dimensional rather than

237   two-dimensional but its presence can be inferred from the hyper-square structure of the ranges.

Modform regions in high dimensions

239   We have implemented the LP algorithm in Eq.9 in an open-source software environment, `modformPRO`. This is writ-

240   ten in Python and exploits Python's linear programming library, PuLP (available from `https://pythonhosted.`

241   `org/PuLP/#`). The software can take as input MS peak-intensity data, or simulated data, for real proteins, construct

242   the corresponding linear equations for the relevant MS experiments (Eq.7), set up the LP problems (Eq.9), call PuLP to

243   solve them and provide the output as ranges for each modform. We chose as an example the human mitogen-activated

244   protein kinase 1 (MAPK1, Erk1, UniProt ID P28482), with all seven phosphorylations reported on UniProt on the

245   sites S29, T185, Y187, T190, S246, S248 and S284, as marked in Table 1. This gives a total of $2^7 = 128$ modforms.

246   This is well below the software's capability but our concern in this paper is not with performance of the algorithm but,

247   rather, what it tells us about high-dimensional modform regions, which are investigated here for the first time. In this

248   respect, 128 dimensions is already considerable and the output can only just be visualised on the printed page.

249   We created two simulated modform distributions for MAPK1 as follows. Consider a phospho-modform as a binary

250   string, where 1 marks the presence of P and 0 marks the absence. The Hamming distance between two modforms is

251   then the number of bits by which they differ. The first simulated distribution ("structured") is one in which the

252   modforms are organised around 4 "modes" with some "noise". Specifically, we chose 4 modforms at random and gave

253   them each a weight of 100. To each modform at Hamming distance 1 from these 4, of which there are 7, we gave a

254   weight of $10u$ where u was a randomly chosen integer between 2 and 8. These are the "modes". For the "noise", we

255   chose 20 modforms at random and gave them weights that were randomly chosen real numbers in $[0, 30]$. If modforms

256   coincided during this procedure, we added up the weights. There should then be nearly 58 modforms with non-zero

257   weights. Finally, we normalised the distribution to the total weight. For the second simulated distribution ("random"),

258   we gave each modform a weight that was a randomly chosen real number in $[0, 100]$ and normalised to the total weight.

259   Although in-vivo data is not yet available, data obtained by in-vitro phosphorylation suggests that modform dis-

260   tributions may be structured, in the sense that few protein modforms arise, despite large numbers of phosphorylated

261   sites [5]. The distinction between the structured and random distributions attempts to reflect this.

262   In `modformPRO`, we computationally specified one experiment on MAPK1 of BU with tryptic digestion followed

11

263 by MS1 on the cleavage peptides and one experiment of TD MS1. Fig.3 shows the range estimations for the structured

264 distribution for each dataset individually and the two datasets combined together. The BU ranges are more variable

265 than the TD ranges, reflecting proteolytic digestion, and they also vary over a broader range, reaching nearly 48% in

266 some cases. However, the average range for BU MS (23.69) is only slightly higher than that for TD MS (22.11). The

267 average range drops much further (16.94) when both datasets are combined.

268 Fig.4 shows the range estimation for the random distribution. Since the experiments are the same, a similar pattern

269 of range variation occurs as for the structured distribution. However, in this case the average range for BU (26.76) is

270 considerably higher than for TD (21.04) and the average range for the combined datasets (18.53) does not improve as

271 much over TD.

272 The exact dimension occupied by the modform region depends on the rank of the matrix M in Eq.7. The rank

273 is readily determined for TD MS1, as the resulting equations use distinct variables and must necessarily be linearly

274 independent. Here, the rank is 8 and the dimension of the modform region for TD is therefore 120. The rank is visible

275 in the block-like arrangement of the TD plots in Fig.3 and 4, in which the ranges fall into a small number of distinct

276 sets. TD MS1 cannot distinguish positional isomers, so we expect from Table 2 that the blocks should follow the

277 binomial distribution on 7 sites: 1 (0P), $2 - 8$ (1P), $9 - 29$ (2P), $30 - 64$ (3P), $65 - 99$ (4P), $100 - 120$ (5P), $121 - 127$

278 (6P) and 128 (7P). Each set of distinct ranges defines a hyper-square like that in Fig.2. 8 hyper-squares are visible

279 for the random distribution but only 7 for the structured. A closer look at the numerical values shows that the 8th

280 hyper-square is present but is visually indistinguishable in the plot. These hyper-squares reveal the polyhedral shape

281 of the modform region in high-dimensions.

282 The rank for BU MS is more delicate. Each peptide arising from proteolytic cleavage gives rise to linearly indepen-

283 dent equations but there are dependencies between the equations from different peptides. We previously determined

284 a formula for the rank for BU MS given any number of proteases and patterns of cleavage [3]. If there is a single

285 protease giving P peptides and peptide i gives rise to e_i equations, then the rank of the equations coming from all the

286 peptides taken together is,

$$\left(\sum_{i=1}^{P} e_i \right) - P + 1 \,.$$

287 Here, proteolytic cleavage of MAPK1 gives 4 peptides with 1, 2, 1 and 3 modifications and, therefore, 2, 3, 2 and 4

288 equations, respectively. Hence, the 11 equations arising from BU have rank $11 - 4 + 1 = 8$. This modform region

289 for BU therefore also has dimension 120. This is harder to see in the BU range estimation because the hyper-square

290 arrangement is shuffled in the modform ordering. For the structured distribution, 7 hyper-squares are visible in the

291 plot and a closer look at the numerical values reveals an 8th. For the random distribution, 6 hyper-squares are visible

292 and no more are found numerically, presumably because they escape numerical resolution.

293 No formula currently exists for the rank of the equations for TD and BU combined, although this is work in

294 progress. We independently determined the rank of the 19 equations to be 14, so that the dimension of the modform

295 region decreases to 104. For the random distribution, we found only 12 hyper-squares, suggesting that the remainder

296 were numerically unresolved. However, for the structured distribution we found 17 hyper-squares. These included

297 2 modforms, the completely unmodified with index 1 and the fully modified with index 128 (Table 2), whose values

298 were exactly determined to be 0. This is not surprising because TD MS1 already accurately accounts for these specific

299 modforms (Fig.3, middle). The larger number of hyper-squares is unexpected, however. It implies the presence of

300 hyper-rectangles, which are defined by more than one distinct range. This indicates that the polyhedral shape of the

301 modform region has become more intricate. Indeed, the dimensions of the hyper-squares are smaller, and there are

302 more hyper-squares with smaller dimensions, for the structured than for the random distribution (Fig.5). The smaller

303 the dimension of the hyper-square, the more constrained are the corresponding variables (Fig.2). We see from Fig.5

304 that the polyhedral shape of the structured modform region is more nuanced and considerably more constrained than

305 that of the random distribution.

DISCUSSION

307 It is evident from Figs.3 and 4 that the ranges estimated by `modformPRO` are quite coarse and do not constrain the

308 actual modform value tightly. However, the purpose of estimating the modform region is not to recover the modform

309 distribution. This is impossible, as we have discussed. Rather, the modform region is the best that can be done, given

310 the available data. The question is, then, what can be learned about such regions using the LP algorithms implemented

311 in `modformPRO`?

312   Modforms regions are defined by the linear equations in Eq.7. The more linearly independent equations that are

313 available, the smaller the dimension of the modform region. It is not surprising, therefore, that combining TD and

314 BU data yields a region of smaller dimension. However, the dimension of a region depends only on the matrix M in

315 Eq.7 and is the same irrespective of the protein and the modform distribution being analysed. The dimension tells us

316 nothing about the size or shape of the region, which depend both on M and on the MS data, which is specified by d

317 in Eq.7 and which represents the modform distribution. We have seen that combining TD with BU data reduces the

318 size, as measured by average modform range, for both the structured and the random distributions. This reiterates the

319 importance of combining MS methods, especially combining those which cleave proteins (BU and MD) with those

320 which do not (TD).

321   The shape of the modform region is also informative. Because modforms regions are defined by linear equations,

322 they are convex and polyhedral but the specific polyhedral shape depends, like the size, on both the matrix M and the

323 data d in Eq.7. The regions that result from BU or from TD have simple polyhedral shape: up to numerical resolution,

324 they consist of hyper-squares, with the number of these being equal to the dimension. The modform region for

13

325 combined TD and BU has a more intricate polyhedral shape and is more constrained (Fig.5), at least for the structured

326 distribution that mimics what might be found in reality [5]. This kind of polyhedral shape is important because it has

327 more degrees of freedom that carry potential information about the modform distribution.

328 We conclude that the LP methods developed here, while offering a coarse approximation to the modform distribu-

329 tion itself, nevertheless provide useful information about the shape of the modform region.

330 This brings us to the critical question of how these methods can be deployed in practice, on real data. This raises

331 two kinds of problems. First, it is necessary for different kinds of dataset to be calibrated with each other. Protocols

332 for undertaking such calibration are being developed. Second, and more intractable, is that there is no independent

333 method for determining the modform distribution. Once data become available, we can apply the methods described

334 here to determine a modform region but how can we know that the actual modform distribution lies within it? The

335 polyhedral shape of the regions offers a potential answer to this conundrum. We may not know where the modform

336 distribution lies but we can ask whether perturbations to the modform distribution give rise to correlated changes in the

337 modform region. The experiments necessary to test such correlations will be easier to undertake in vitro, by titrating

338 the levels of modification or demodification enzymes [5]. (Similar perturbations can be carried out in vivo but may

339 have unpredictable effects through indirect or feedback connections within the network of enzymes.) The effect of

340 such perturbations on the modform distribution can be reasonably well predicted and the consequent impact on the

341 modform region calculated. If that change is seen in the data, it would confirm that the shape of the modform region is

342 acting as a proxy for the modform distribution. Such experimental tests are the next step towards practical exploitation

343 of modform regions and the LP algorithms introduced here.

Author Contributions

345 DA designed and wrote the software, with the help of RTF, BPE, DL, CJD, PDC and PMT. RTF and BPE implemented

346 the public distribution and undertook the data analysis. GL, NLK and JG conceived the project. JG wrote the paper

347 with the help of all co-authors.

Acknowledgments

References

[1] R. Aebersold, J. N. Agar, I. J. Amster, M. S. Baker, C. R. Bertozzi, E. S. Boja, C. E. Costello, B. F. Cravatt, C. Fenselau, B. A. Garcia, Y. Ge, J. Gunawardena, R. C. Hendrickson, P. J. Hergenrother, C. G. Huber, A. R. Ivanov, O. N. Jensen, M. C. Jewett, N. L. Kelleher, L. L. Kiessling, N. J. Krogan, M. R. Larsen, J. A. Loo, R. R. Ogorzalek Loo, E. Lundberg, M. J. MacCoss, P. Mallick, V. K. Mootha, M. Mrksich, T. W. Muir, S. M. Patrie, J. J. Pesavento, S. J. Pitteri, H. Rodriguez, A. Saghatelian, W. Sandoval, H. Schlüter, S. Sechi, S. A. Slavoff, L. M. Smith, M. P. Snyder, P. M. Thomas, M. Uhlén, J. E. Van Eyk, M. Vidal, D. R. Walt, F. M. White, E. R. Williams, T. Wohlschlager, V. H. Wysocki, N. A. Yates, N. L. Young, and B. Zhang. How many human proteoforms are there? *Nat. Chem. Biol.*, 14:206–14, 2018.

[2] B. A. Benayoun and R. A. Veitia. A post-translational modification code for transcription factors: sorting through a sea of signals. *Trends Cell Biol.*, 19:189–97, 2009.

[3] P. D. Compton, N. L. Kelleher, and J. Gunawardena. Estimating the distribution of protein post-translational modification states by mass spectrometry. *J. Proteome. Res.*, 17:2727–34, 2018.

[4] C. J. DeHart, J. S. Chahal, S. J. Flint, and D. H. Perlman. Extensive post-translational modification of active and inactivated forms of endogenous p53. *Mol. Cell. Proteomics*, 13:1–17, 2014.

[5] C. J. DeHart, L. Fornelli, L. C. Anderson, R. T. Fellers, D. Lu, C. L. Hendrickson, G. Lahav, J. Gunawardena, and N. L. Kelleher. A multi-modal proteomics strategy for characterizing posttranslational modifications of tumor suppressor p53 reveals many sites but few modified forms. bioRxiv `doi:10.1101/455527`, 2018.

[6] S. Egloff and S. Murphy. Cracking the RNA polymerase II CTD code. *Trends Genet.*, 24:260–8, 2008.

[7] T. M. Filtz, W. K. Vogel, and M. Leid. Regulation of transcription factor activity by interconnected posttranslational modifications. *Trends Pharmacol. Sci.*, 35:76–85, 2014.

[8] T. Jenuwein and C. D. Allis. Translating the histone code. *Science*, 293:1074–80, 2001.

[9] P. Korkuć and D. Walther. Towards understanding the crosstalk between protein post-translational modifications: homo- and heterotypic PTM pair distances on protein surfaces are not random. *Proteins*, 85:78–92, 2017.

[10] I. Landrieu, A. Leroy, C. Smet-Nocca, I. Huvent, L. Amniai, M. Hamdane, N. Sibille, L. Buée, J.-M. Wieruszeski, and G. Lippens. NMR spectroscopy of the neuronal tau protein: normal function and implication in alzheimerâĂŹs disease. *Biochem. Soc. Trans.*, 38:1006–11, 2010.

[11] J.-S. Lee, E. Smith, and A. Shilatifard. The language of histone crosstalk. *Cell*, 142:682–5, 2010.

379 [12] G. Lippens, E. Cahoreau, P. Millard, C. Charlier, J. Lopez, X. Hanoulle, and J. C. Portais. In-cell NMR: from
380   metabolites to macromolecules. *Analyst*, 143:620–9, 2018.

381 [13] D. C. Love and J. A. Hanover. The hexosamine signaling pathway: deciphering the 'O-GlcNAc code'. *Sci STKE*,
382   312:re13, 2005.

383 [14] P. Miguez, I. Letunic, L. Parca, and P. Bork. PTMcode: a database of known and predicted functional associations
384   between post-translational modifications in proteins. *Nucleic Acids Res.*, 41:D306–11, 2012.

385 [15] F. Murray-Zmijewski, E. A. Shue, and X. Lu. A complex barcode underlies the heterogeneous response of p53
386   to stress. *Nat. Rev. Mol. Cell Biol.*, 9:702–12, 2008.

387 [16] K. M. Nobles, K. Xiao, S. Ahn, A. K. Shukla, C. M. Lam, S. Rajagopal, R. T. Strachan, T.-Y. Huang, E. A.
388   Bressler, M. R. Hara, S. K. Shenoy, S. P. gygi, and R. J. Lefkowitz. Distinct phosphorylation sites on the β_2
389   adrenergic receptor establish a barcode that encodes differential functions of β-arrestin. *Sci. Signal.*, 4:ra51,
390   2011.

391 [17] B. W. O'Malley, J. Qin, and R. B. Lanz. Cracking the coregulator codes. *Curr. Opin. Cell Biol.*, 20:310–5, 2008.

392 [18] S. Prabakaran, R. A. Everley, I. Landrieu, J. M. Wieruszeski, G. Lippens, H. Steen, and J. Gunawardena. Com-
393   parative analysis of Erk phosphorylation suggests a mixed strategy for measuring phospho-form distributions.
394   *Mol. Syst. Biol.*, 7:482, 2011.

395 [19] S. Prabakaran, G. Lippens, H. Steen, and J. Gunawardena. Post-translational modification: nature's escape from
396   from genetic imprisonment and the basis for cellular information processing. *Wiley Interdiscip. Rev. Syst. Biol.*
397   *Med.*, 4:565–83, 2012.

398 [20] V. Schwämmle, S. Sidoli, C. Ruminowicz, X. Wu, C.-F. Lee, K. Helin, and O. N. Jensen. Systems level analysis
399   of histone H3 posttranslational modifications (PTMs) reveals features of PTM crosstalk in chromatin regulation.
400   *Mol. Cell. Proteom.*, 15:2715–29, 2016.

401 [21] A. Shevchenko, H. Tomas, J. Havlis, J. V. Olsen, and M. Mann. In-gel digestion for mass spectrometric charac-
402   terization of proteins and proteomes. *Nat. Protoc.*, 1:2856–60, 2006.

403 [22] T. K. Toby, L. Fornelli, and N. L. Kelleher. Progress in top-down proteomics and the analysis of proteoforms.
404   *Annu. Rev. Anal. Chem.*, 9:499–519, 2016.

405 [23] L. Tsiatsiani and A. J. Heck A. Proteomics beyond trypsin. *FEBS J.*, 282:2612–26, 2015.

406 [24] B. Turner. Cellular memory and the histone code. *Cell*, 111:285–91, 2002.

407   [25] A. S. Venne, L. Kollipara, and R. P. Zahedi. The next level of complexity: crosstalk of posttranslational modifi-

408   cations. *Proteomics*, 14:513–24, 2014.

409   [26] K. J. Verhey and J. Gaertig. The tubulin code. *Cell Cycle*, 6:2152–60, 2007.

410   [27] C. T. Walsh. *Posttranslational Modification of Proteins*. Roberts and Company, Englewood, Colorado, 2006.

	10	20	30	40	50
	MAAAAAAGAG	PEMVRGQVFD	VGPRYTNL**S**Y	IGEGAYGMVC	SAYDNVNKVR
	60	70	80	90	100
	VAIKKISPFE	HQTYCQRTLR	EIKILLRFRH	ENIIGINDII	RAPTIEQMKD
	110	120	130	140	150
	VYIVQDLMET	DLYKLLKTQH	LSNDHICYFL	YQILRGLKYI	HSANVLHRDL
	160	170	180	190	200
	KPSNLLLNTT	CDLKICDFGL	ARVADPDHDH	TGFL**TEY**VA**T**	RWYRAPEIML
	210	220	230	240	250
	NSKGYTKSID	IWSVGCILAE	MLSNRPIFPG	KHYLDQLNHI	LGILG**S**P**S**QE
	260	270	280	290	300
	DLNCIINLKA	RNYLLSLPHK	NKVPWNRLFP	NAD**S**KALDLL	DKMLTFNPHK
	310	320	330	340	350
	RIEVEQALAH	PYLEQYYDPS	DEPIAEAPFK	FDMELDDLPK	EKLKELIFEE
	360				
	TARFQPGYRS				

Table 1: MAPK1 amino-acid sequence for UniProt P28482. The seven phosphorylatable residues annotated in UniProt and used in this study are shown in blue.

1	0	61	S28P.Y186P.S245P	121	S28P.T184P.Y186P.T189P.S245P.S247P
2	T189P	62	Y186P.S245P.S283P	122	T184P.Y186P.T189P.S245P.S247P.S283P
3	S247P	63	S28P.S245P.S283P	123	S28P.T184P.T189P.S245P.S247P.S283P
4	T184P	64	S28P.Y186P.S283P	124	S28P.T184P.Y186P.T189P.S247P.S283P
5	S245P	65	T184P.T189P.S245P.S247P	125	S28P.Y186P.T189P.S245P.S247P.S283P
6	Y186P	66	T184P.Y186P.T189P.S247P	126	S28P.T184P.Y186P.T189P.S245P.S283P
7	S28P	67	S28P.T184P.T189P.S247P	127	S28P.T184P.Y186P.S245P.S247P.S283P
8	S283P	68	T184P.T189P.S247P.S283P	128	S28P.T184P.Y186P.T189P.S245P.S247P.S283P
9	T189P.S247P	69	Y186P.T189P.S245P.S247P		
10	T184P.T189P	70	S28P.T189P.S245P.S247P		
11	T189P.S245P	71	T189P.S245P.S247P.S283P		
12	Y186P.T189P	72	S28P.Y186P.T189P.S247P		
13	S28P.T189P	73	Y186P.T189P.S247P.S283P		
14	T189P.S283P	74	S28P.T189P.S247P.S283P		
15	T184P.S247P	75	T184P.Y186P.T189P.S245P		
16	S245P.S247P	76	S28P.T184P.T189P.S245P		
17	Y186P.S247P	77	T184P.T189P.S245P.S283P		
18	S28P.S247P	78	S28P.T184P.Y186P.T189P		
19	S247P.S283P	79	T184P.Y186P.T189P.S283P		
20	T184P.S245P	80	S28P.T184P.T189P.S283P		
21	T184P.Y186P	81	S28P.Y186P.T189P.S245P		
22	S28P.T184P	82	Y186P.T189P.S245P.S283P		
23	T184P.S283P	83	S28P.T189P.S245P.S283P		
24	Y186P.S245P	84	S28P.Y186P.T189P.S283P		
25	S28P.S245P	85	T184P.Y186P.S245P.S247P		
26	S245P.S283P	86	S28P.T184P.S245P.S247P		
27	S28P.Y186P	87	T184P.S245P.S247P.S283P		
28	Y186P.S283P	88	S28P.T184P.Y186P.S247P		
29	S28P.S283P	89	T184P.Y186P.S247P.S283P		
30	T184P.T189P.S247P	90	S28P.T184P.S247P.S283P		
31	T189P.S245P.S247P	91	S28P.Y186P.S245P.S247P		
32	Y186P.T189P.S247P	92	Y186P.S245P.S247P.S283P		
33	S28P.T189P.S247P	93	S28P.S245P.S247P.S283P		
34	T189P.S247P.S283P	94	S28P.Y186P.S247P.S283P		
35	T184P.T189P.S245P	95	S28P.T184P.Y186P.S245P		
36	T184P.Y186P.T189P	96	T184P.Y186P.S245P.S283P		
37	S28P.T184P.T189P	97	S28P.T184P.S245P.S283P		
38	T184P.T189P.S283P	98	S28P.T184P.Y186P.S283P		
39	Y186P.T189P.S245P	99	S28P.Y186P.S245P.S283P		
40	S28P.T189P.S245P	100	T184P.Y186P.T189P.S245P.S247P		
41	T189P.S245P.S283P	101	S28P.T184P.T189P.S245P.S247P		
42	S28P.Y186P.T189P	102	T184P.T189P.S245P.S247P.S283P		
43	Y186P.T189P.S283P	103	S28P.T184P.Y186P.T189P.S247P		
44	S28P.T189P.S283P	104	T184P.Y186P.T189P.S247P.S283P		
45	T184P.S245P.S247P	105	S28P.T184P.T189P.S247P.S283P		
46	T184P.Y186P.S247P	106	S28P.Y186P.T189P.S245P.S247P		
47	S28P.T184P.S247P	107	Y186P.T189P.S245P.S247P.S283P		
48	T184P.S247P.S283P	108	S28P.T189P.S245P.S247P.S283P		
49	Y186P.S245P.S247P	109	S28P.Y186P.T189P.S247P.S283P		
50	S28P.S245P.S247P	110	S28P.T184P.Y186P.T189P.S245P		
51	S245P.S247P.S283P	111	T184P.Y186P.T189P.S245P.S283P		
52	S28P.Y186P.S247P	112	S28P.T184P.T189P.S245P.S283P		
53	Y186P.S247P.S283P	113	S28P.T184P.Y186P.T189P.S283P		
54	S28P.S247P.S283P	114	S28P.Y186P.T189P.S245P.S283P		
55	T184P.Y186P.S245P	115	S28P.T184P.Y186P.S245P.S247P		
56	S28P.T184P.S245P	116	T184P.Y186P.S245P.S247P.S283P		
57	T184P.S245P.S283P	117	S28P.T184P.S245P.S247P.S283P		
58	S28P.T184P.Y186P	118	S28P.T184P.Y186P.S247P.S283P		
59	T184P.Y186P.S283P	119	S28P.Y186P.S245P.S247P.S283P		
60	S28P.T184P.S283P	120	S28P.T184P.Y186P.S245P.S283P		

Table 2: Indices and modforms for the MAPK1 example. Indices are chosen internally by modformPRO.
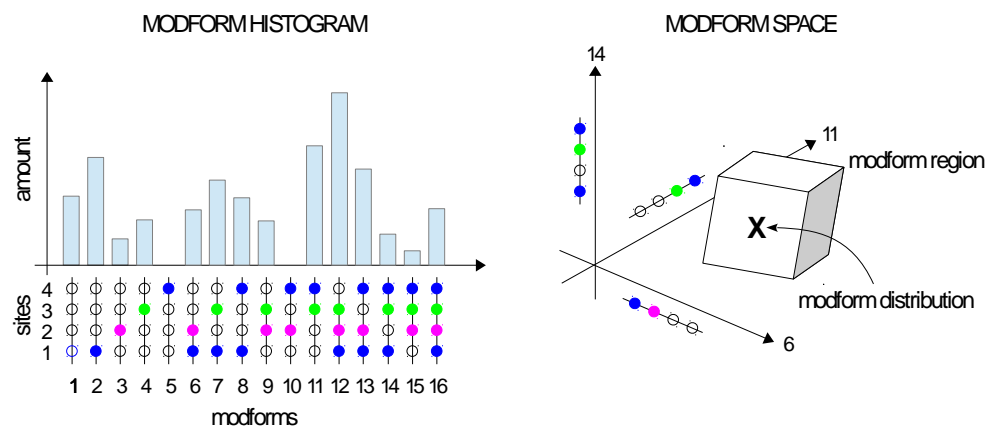
19

Figure 1: Modforms, distributions and regions. A hypothetical modform distribution is shown as a histogram (left). The protein has 3 types of PTM (blue, magenta, green) at 4 sites, giving 16 modforms in total. The modform distribution can also be viewed as a point (X) in a sixteen-dimensional space (right), where only the three dimensions corresponding to modforms 6, 11 and 14 are shown. Mass-spectrometry data give rise to linear equations which constrain the modform distribution to lie within a modform region (box).
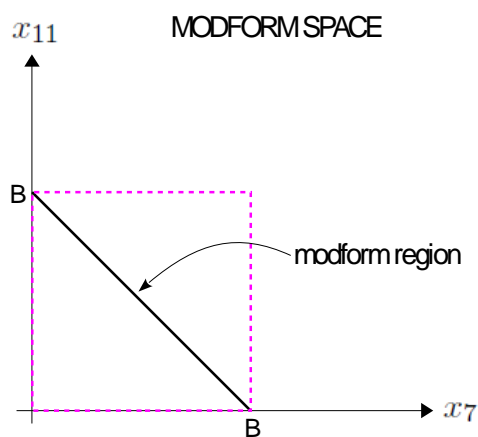
Figure 2: Modform range determination by linear programming (LP). The modform region (black segment) of the linear system given by Eq.7 is shown, in the space of modforms 7 and 11. The ranges obtained by solving the LP problem in Eq.9 gives the same result as if the modform region were the "hyper-square" with magenta dashes.
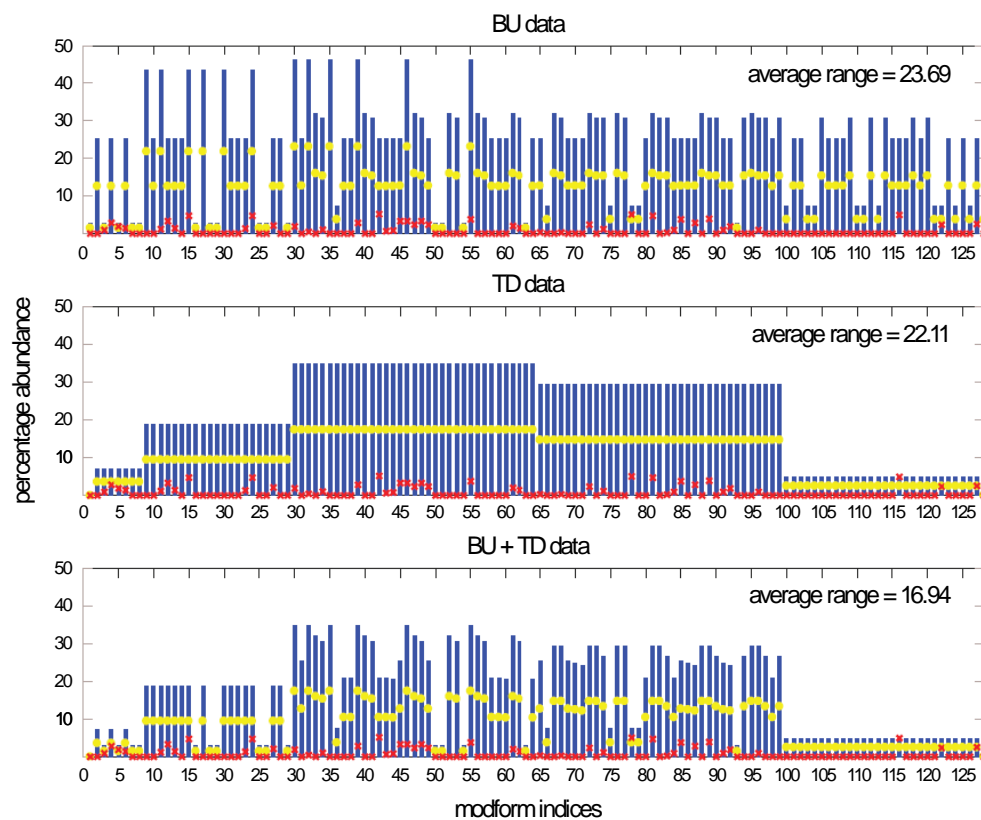
20

Figure 3: `modformPRO` output for the structured distribution. The modforms corresponding to the indices are shown in Table 2. Red crosses mark the actual values of the modform distribution; blue bars show the range estimated by LP from Eq.9; yellow discs mark the midpoint of each range. The average range is calculated over all 128 modforms.
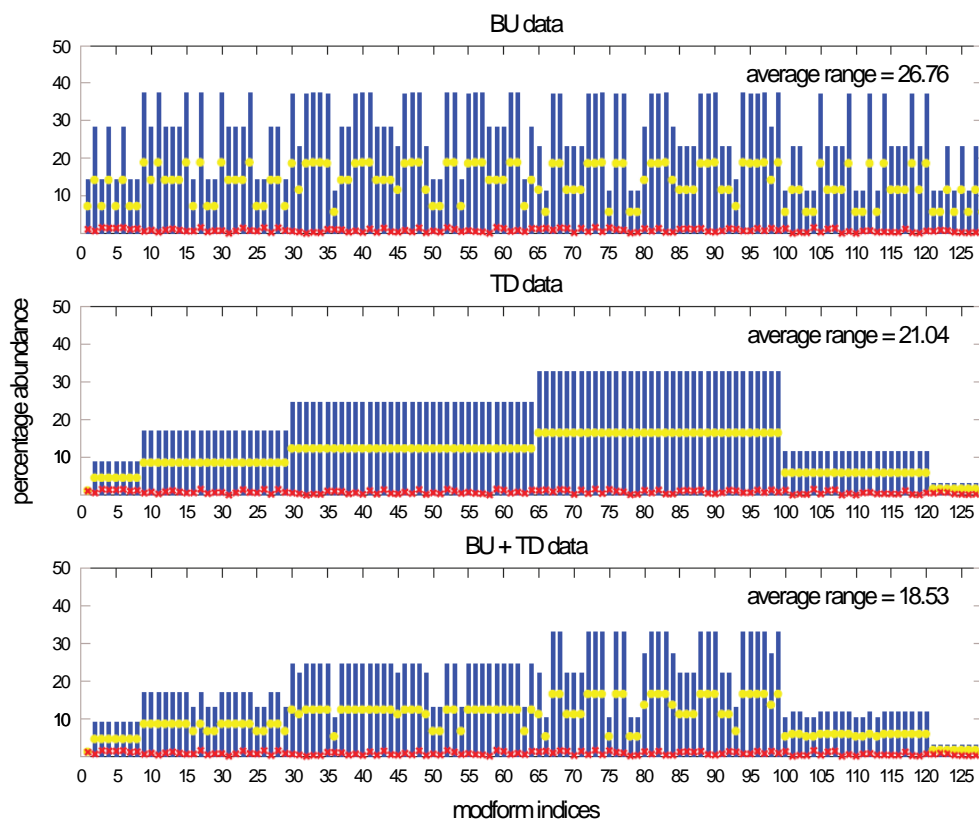
Figure 4: `modformPRO` output for the random distribution, following the same conventions as in Fig.3. Because of the way weights were chosen for this distribution, as explained in the text, the normalised values (red crosses) must each be below 0.8.
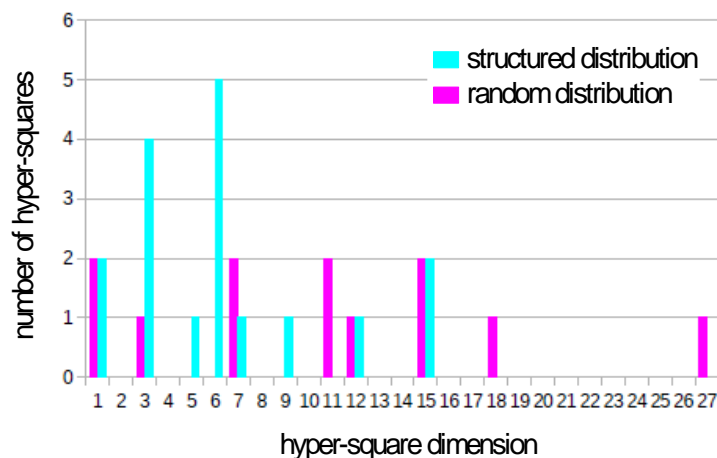

Figure 5: Histogram showing the frequency of hyper-square dimensions arising from combined TD and BU MS, determined from the range estimations for the structured distribution (Fig.3 bottom plot, cyan) and the random distribution (Fig.4 bottom plot, magenta).

22